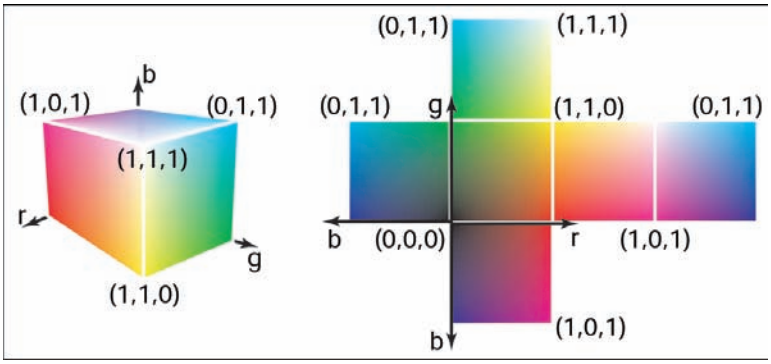

Plate I. The RGB color cube in 3D and its faces unfolded. Any RGB color is a point in the cube. (See also Figure 3.13.)

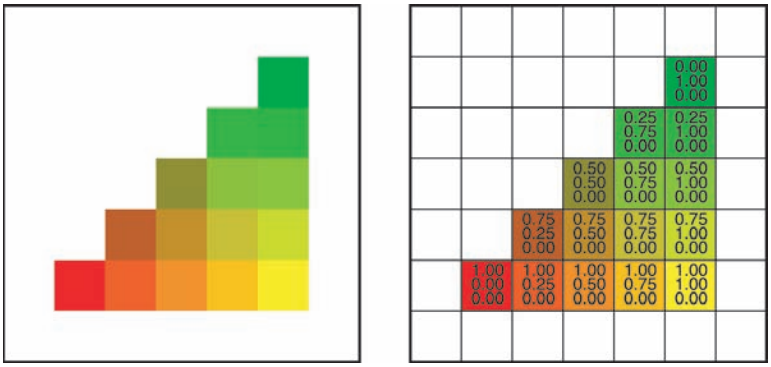

Plate II. A colored triangle with barycentric interpolation. Note that the changes in color components are linear in each row and column as well as along each edge. In fact it is constant along every line, such as the diagonals, as well. (See also Figure 8.5.)

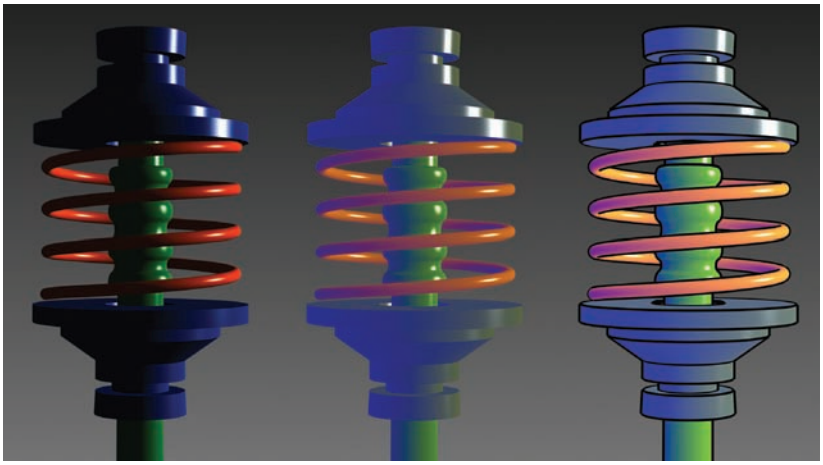

Plate III. Left: a Phong-illuminated image. Middle: cool-to-warm shading is not useful without silhouettes. Right: cool-to-warm shading plus silhouettes. *Image courtesy Amy Gooch.* (See also Figure 10.9.)

Plate IV. The color of the glass is affected by total internal reflection and Beer's Law. The amount of light transmitted and reflected is determined by the Fresnel Equations. The complex lighting on the ground plane was computed using particle tracing as described in Chapter 24. (See also Figure 13.3.)

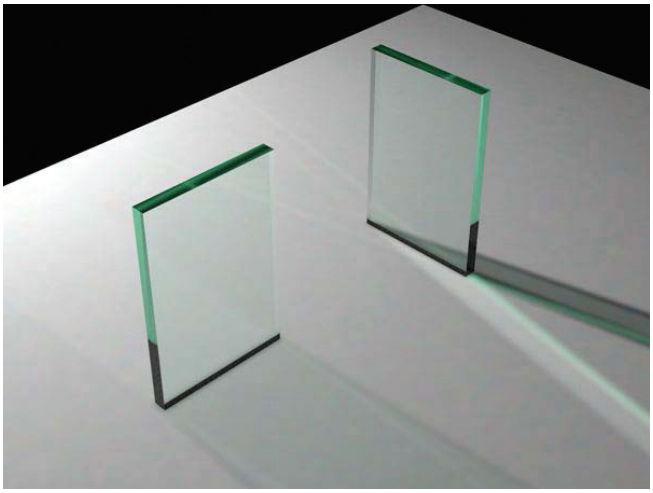

Plate V. An example of depth of field. The caustic in the shadow of the wine glass is computed using particle tracing (Chapter 24). (See also Figure 13.16.)

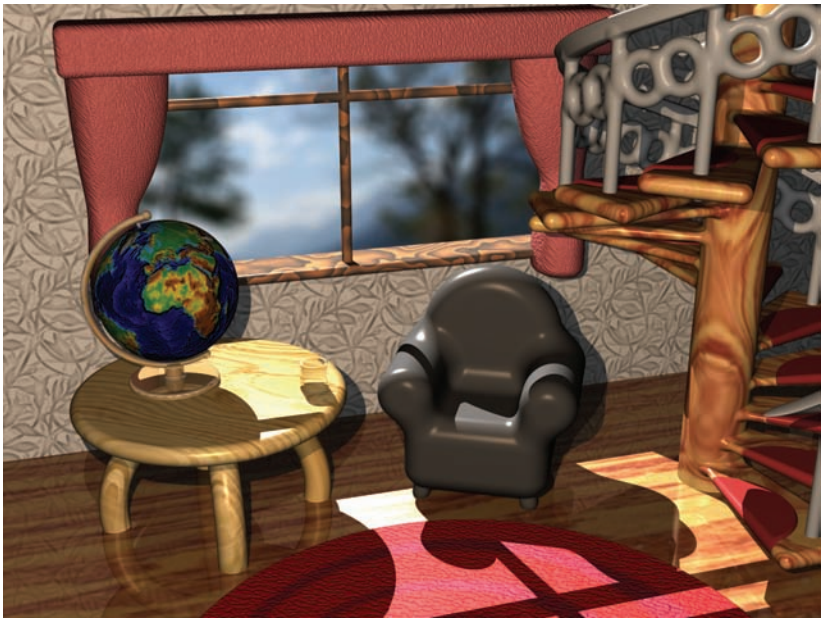

Plate VI. "Spiral Stairs." A complex BlobTree implicit model created in Erwin DeGroot's BlobTree.net system. (See also Figure 16.28.)

Plate VII. "The Next Step." A complex BlobTree implicit model created interactively in Ryan Schmidt's Shapeshop by artist, Corien Clapwijk (Andusan). (See also Figure 16.31.)

Plate VIII. Each sphere is rendered using only a vertex shader that computes Phong shading. Because the computation is being performed on a per-vertex basis, the Phong highlight only begins to appear accurate after the amount of geometry used to model the sphere is increased drastically. (See also Figure 18.7.)

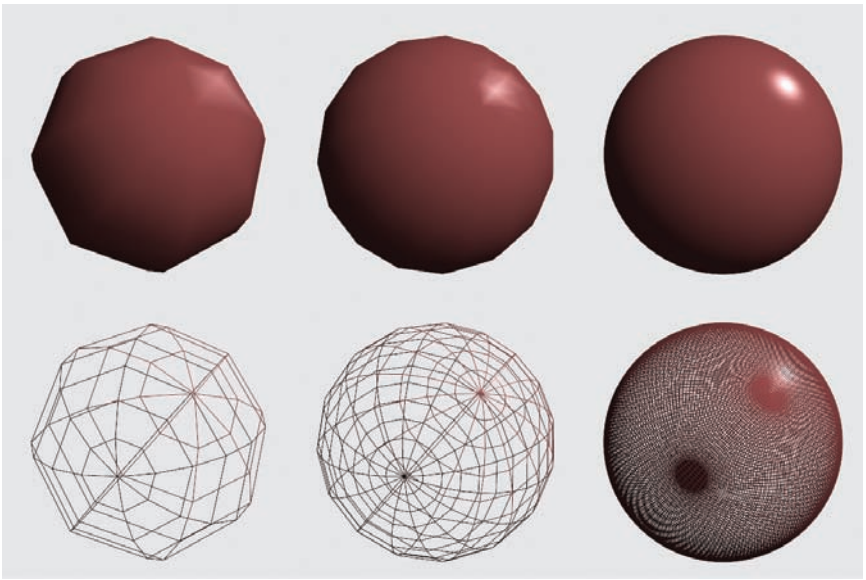

Plate IX. The results of running the fragment shader from Section 18.3.4. Note that the Phong highlight does appear on the left-most model which is represented by a single polygon. In fact, because lighting is calculated at the fragment, rather than at each vertex, the more coarsely tessellated sphere models also demonstrate appropriate Phong shading. (See also Figure 18.8.)

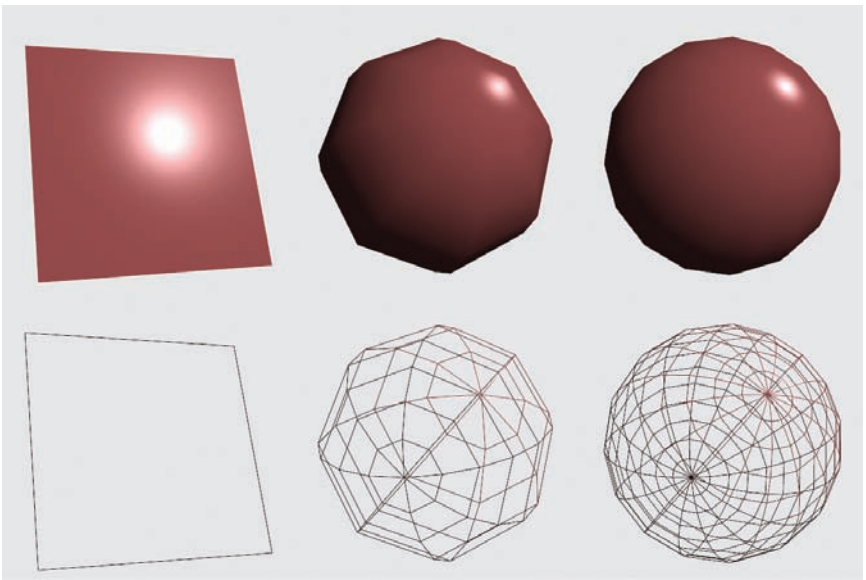

Plate X. The visible spectrum. Wavelengths are in nanometers.

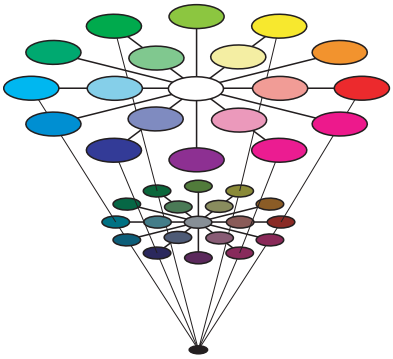

Plate XI. HSV color space. Hue varies around the circle, saturation varies with radius, and value varies with height.

Plate XII. Which color is closer to red: green or violet?

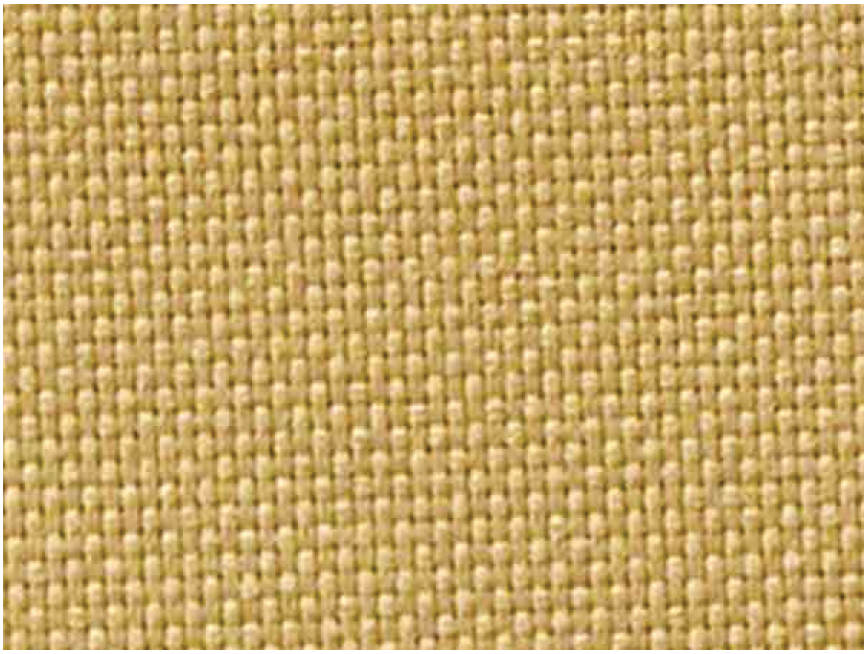

Plate XIII. The effect shown in Figure 22.29 is even more powerful when shown in color. *Figure courtesy Albert Yonas.*

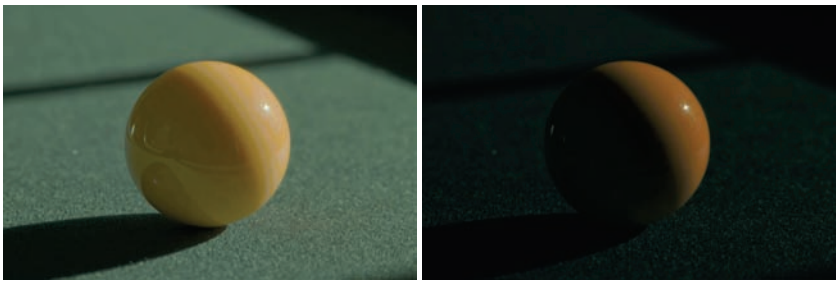

Plate XIV. Per-channel gamma correction may desaturate the image. The left image was desaturated with a value of $s = 0.5$. The right image was not desaturated ($s = 1$). (See also Figure 23.11.)

Plate XV. Image used for demonstrating the color transfer technique. Results are shown in Color Plates XVI and XVIII. (See also Figure 23.12 and Figure 23.30.)

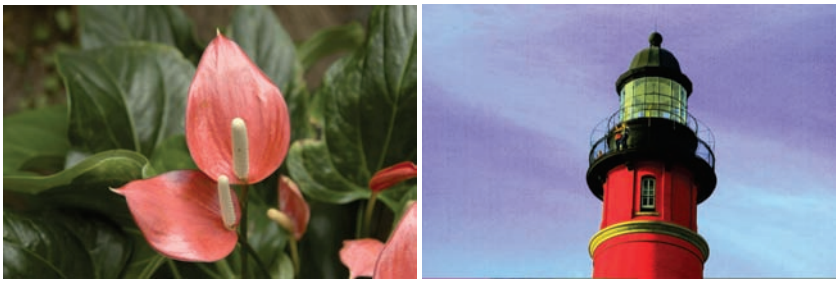

Plate XVI. The image on the left is used to adjust the colors of the image shown in Color Plate XV. The result is shown on the right. (See also Figure 23.13.)

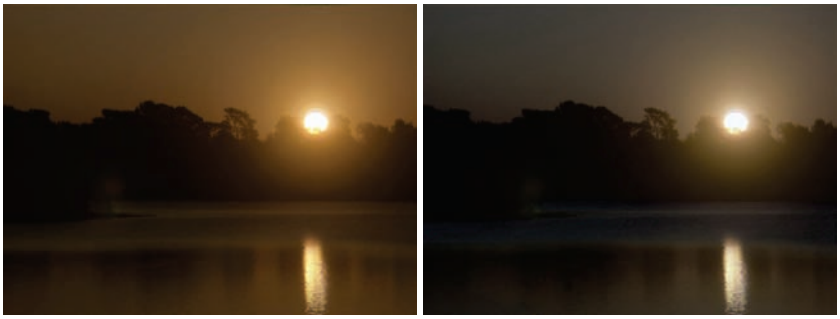

Plate XVII. Linear interpolation for color correction. The parameter c is set to 0.0 in the left image and to 1.0 in the right image. (See also Figure 23.24.)

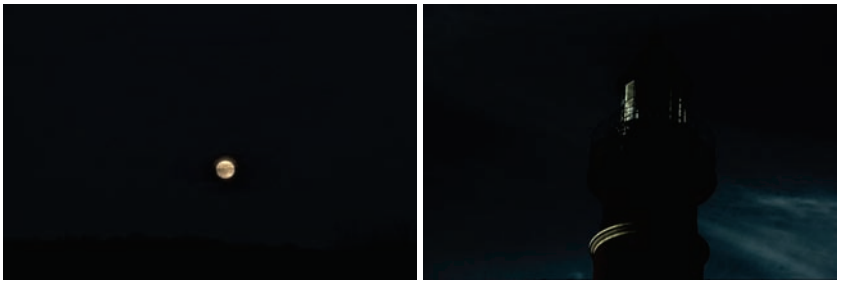

Plate XVIII. The image on the left is used to transform the image of Color Plate XV into a night scene, shown here on the right. (See also Figure 23.31.)

Plate XIX. Simulated night scene using the image shown in Color Plate XV. (See also Figure 23.30.)

Plate XX. Aerial perspective, in which atmospheric effects reduce contrast and shift colors towards blue, provides a depth cue over long distances.

Plate XXI. A comparison between a rendering and a photo. *Figure courtesy Sumant Pattanaik and the Cornell Program of Computer Graphics.* (See also Figure 24.9.)

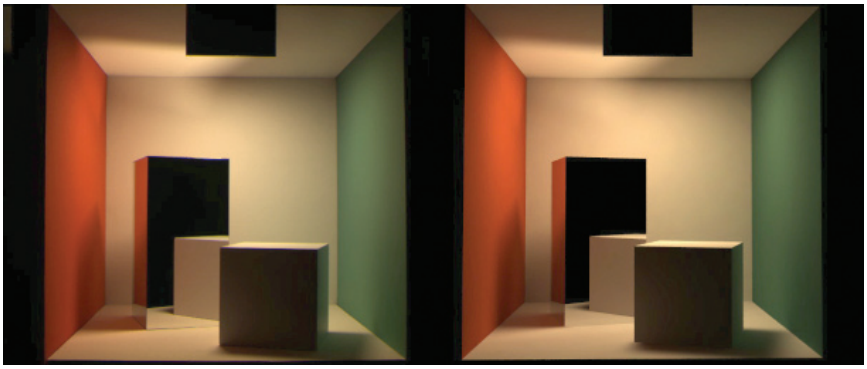

Plate XXII. The image shows extreme motion blur effects. The shadows use distribution ray tracing because they are moving during the image. *Model by Joseph Hamdorf and Young Song. Rendering by Eric Levin.*

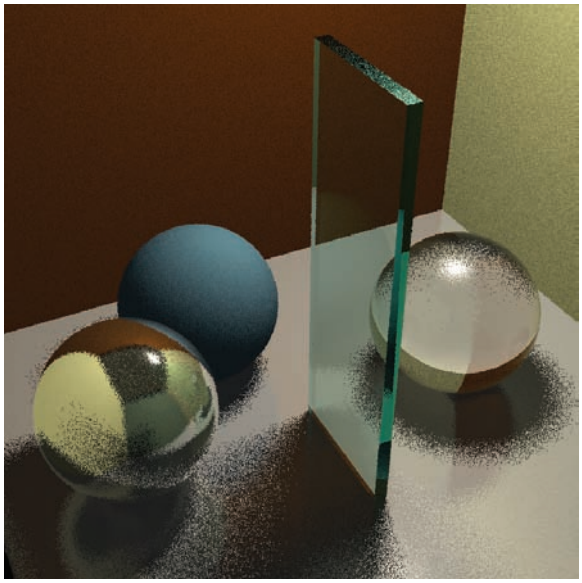

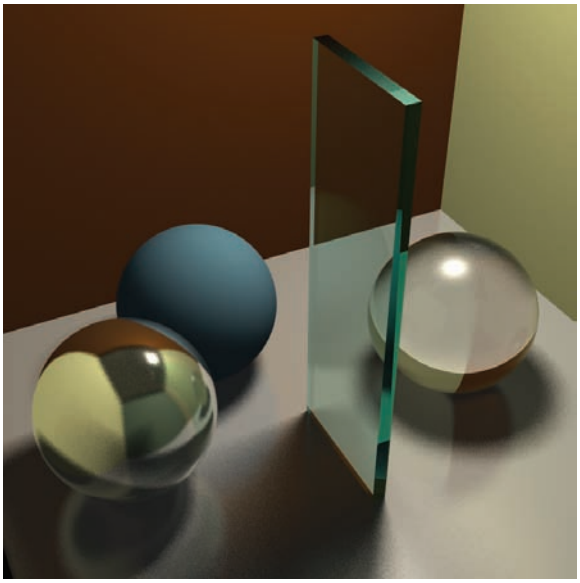

Plate XXIII. Distribution ray-traced images with 1 sample per pixel, 16 samples per pixel, and 256 samples per pixel. *Images courtesy Jason Waltman.*

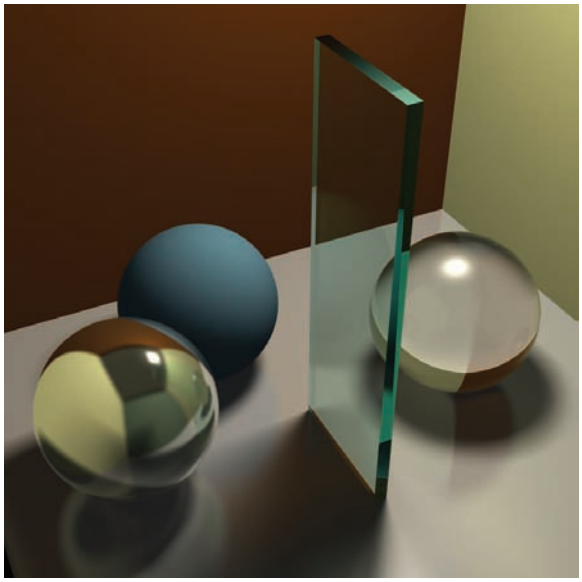

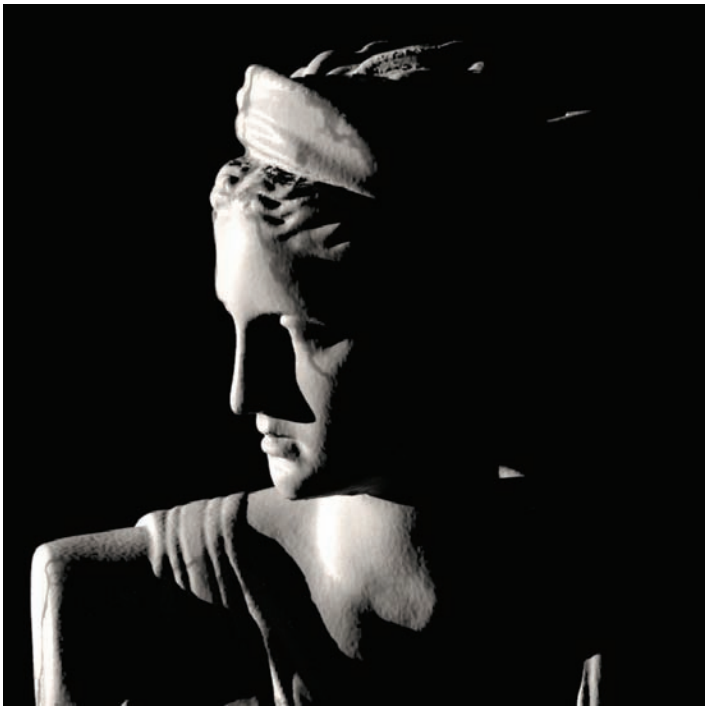

Plate XXIV. Top: A diffuse shading model is used. Bottom: Subsurface scattering is allowed using a technique from “A Practical Model for Sub-surface Light Transport,” Jensen et al., Proceedings of SIGGRAPH 2001. *Images courtesy Henrik Jensen.*

Plate XXV. Ray-traced and photon-mapped image of an interior. Most of the lighting is indirect. *Image courtesy Henrik Jensen.*

Plate XXVI. The brightly colored pattern in the shadow is a “caustic” and is a product of light focused through the glass. It was computed using photon tracing. *Image courtesy Henrik Jensen.*

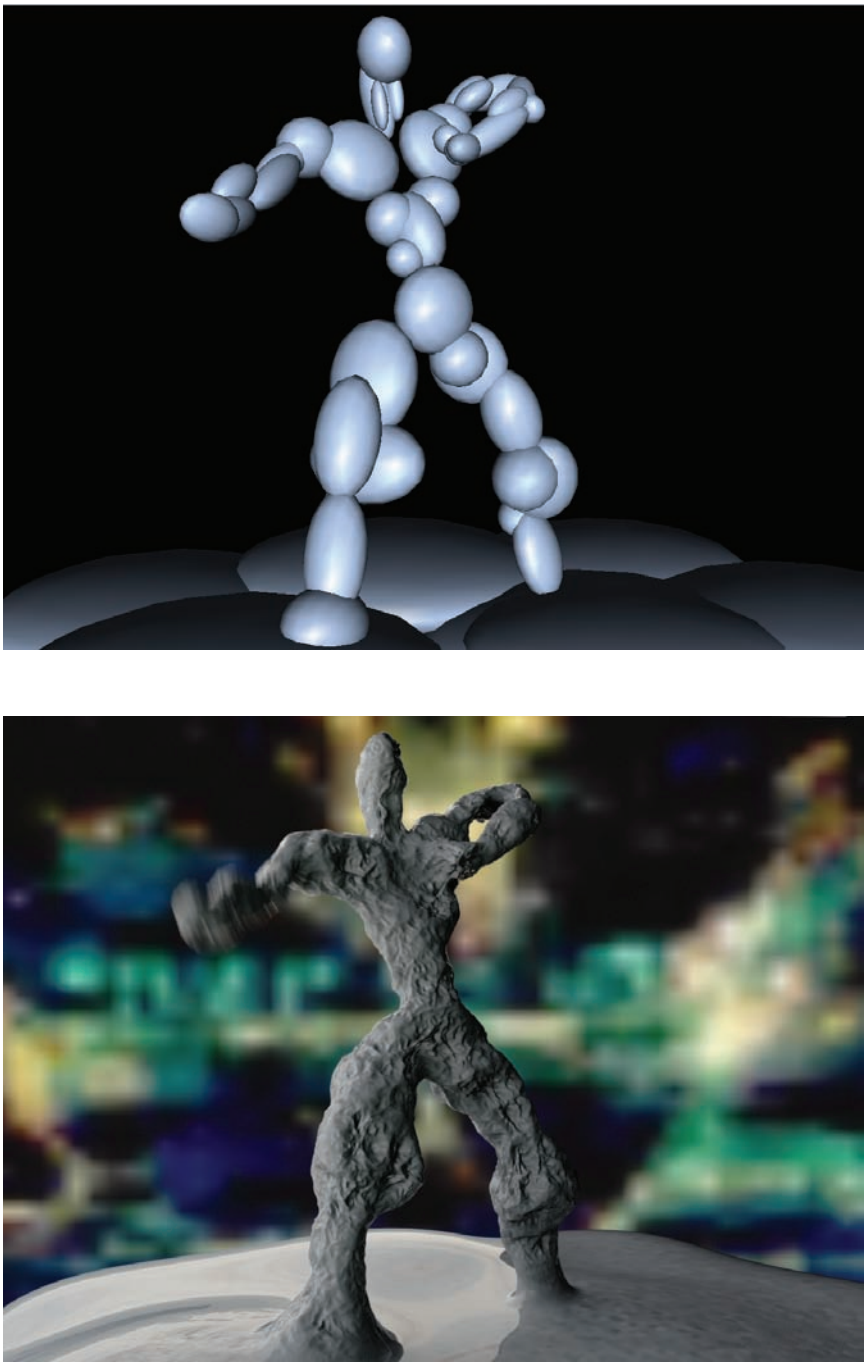

Plate XXVII. Top: A set of ellipsoids approximates the model. Bottom: The ellipsoids are used to create a gravity-like implicit function which is then displaced. *Image courtesy Eric Levin.*

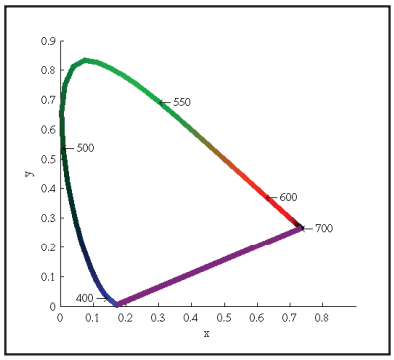

Plate XXVIII. The spectrum locus for the CIE 1931 standard observer. (See also Figure 21.6).

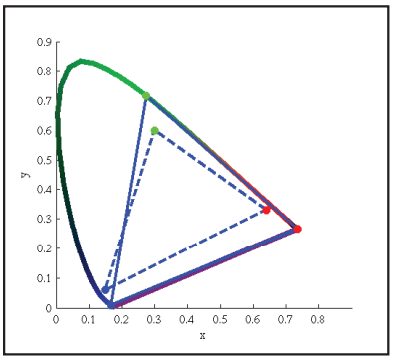

Plate XXIX. The chromaticity boundaries of the CIE RGB primaries at 435.8, 546.1, and 700 nm (solid) and a typical HDTV (dashed). (See also Figure 21.7.)

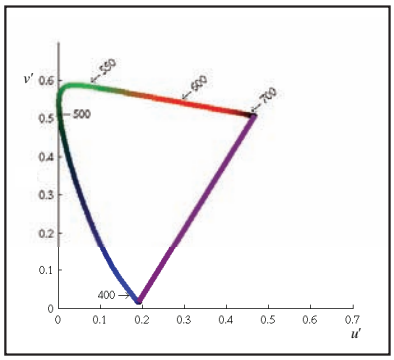

Plate XXX. The CIE $u'v'$ chromaticity diagram. (See also Figure 21.8.)

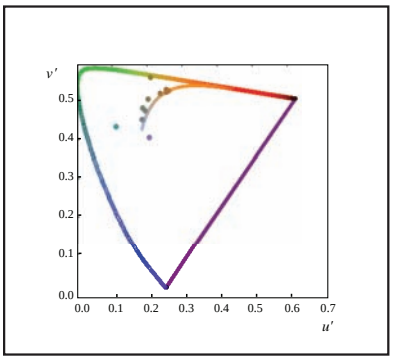

Plate XXXI. A series of light sources plotted in the CIE $u'v'$ chromaticity diagram. A white piece of paper illuminated by any of these light sources maintains a white color appearance. (See also Figure 21.11.)

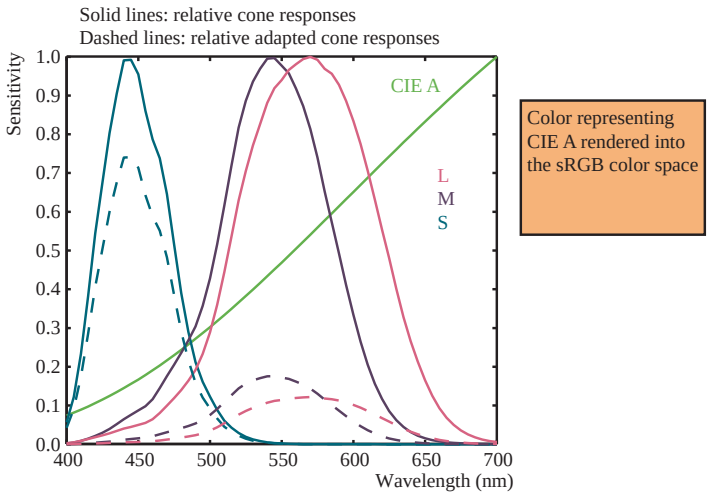

Color representing CIE A rendered into the sRGB color space

Plate XXXII. An example of von Kries–style independent photoreceptor gain control. The relative cone responses (solid line) and the relative adapted cone responses to CIE illuminant A (dashed) are shown. The separate patch of color represents CIE illuminant A rendered into the sRGB color space. (See also Figure 21.12.)

Plate XXXIII. *Crysis* exemplifies the realistic and detailed graphics expected of first-person shooters. *Image courtesy Crytek.* (See also Figure 26.2.)

Plate XXXIV. An example of highly stylized, non-photorealistic rendering from the game *Okami*. *Image courtesy Capcom Entertainment, Inc.* (See also Figure 26.3.)

Plate XXXV. The *LittleBigPlanet* developers took care to choose techniques that fit the game's constraints, combining them in unusual ways to achieve stunning results. *LittleBigPlanet* © *2007 Sony Computer Entertainment Europe. Developed by Media Molecule. LittleBigPlanet is a trademark of Sony Computer Entertainment Europe.* (See also Figure 26.4.)

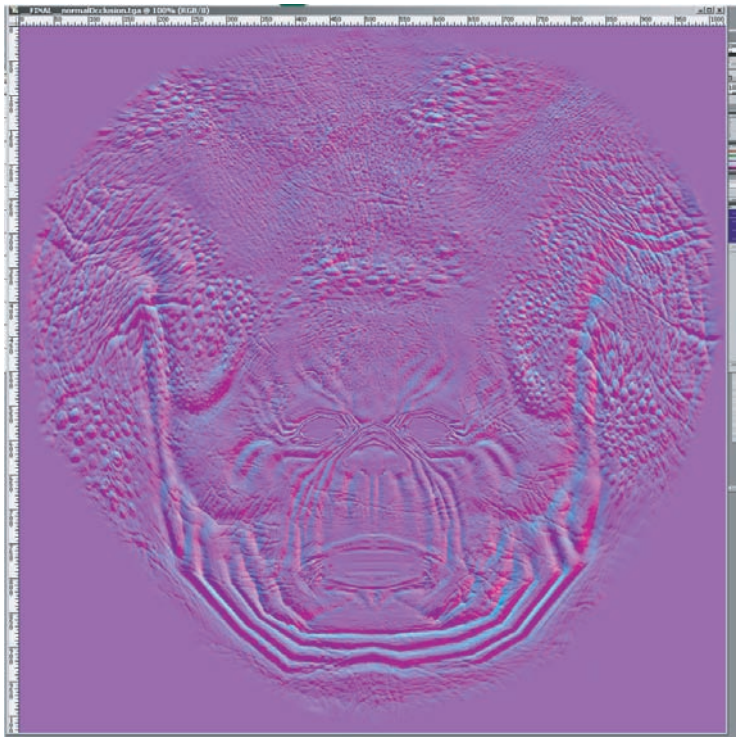

Plate XXXVI. The normal map used in Figure 26.8. In this image, the red, green and blue channels of the texture contain the X, Y, and Z coordinates of the surface normals. *Image courtesy Keith Bruns.* (See also Figure 26.9.)

Plate XXXVII. An early version of a diffuse color texture for the mesh from Figure 26.8, shown in Photoshop. *Image courtesy Keith Bruns.* (See also Figure 26.10.)

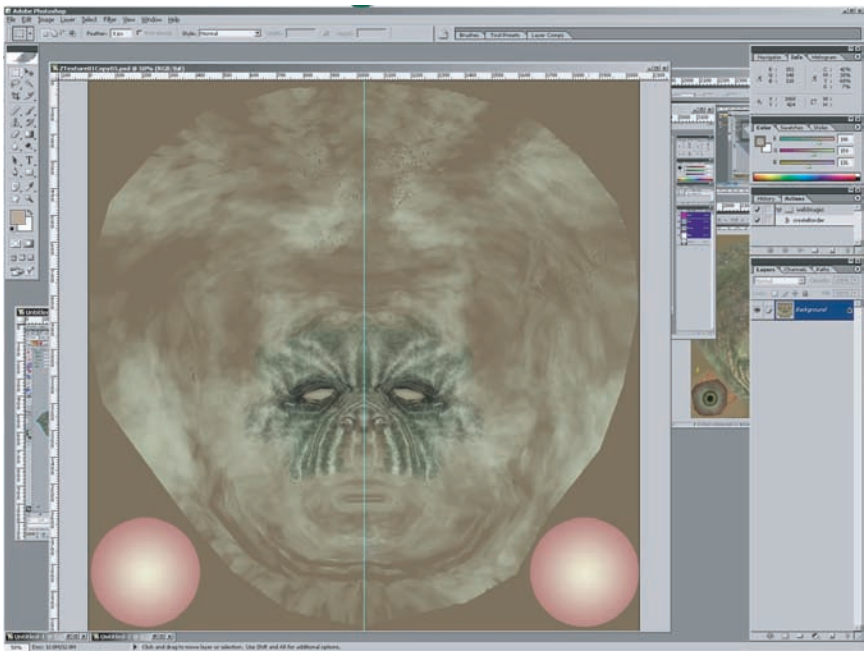

Plate XXXVIII. A rendering (in ZBrush) of the mesh with normal map and early diffuse color texture (from Plate XXXVII) applied. *Image courtesy Keith Bruns.* (See also Figure 26.11.)

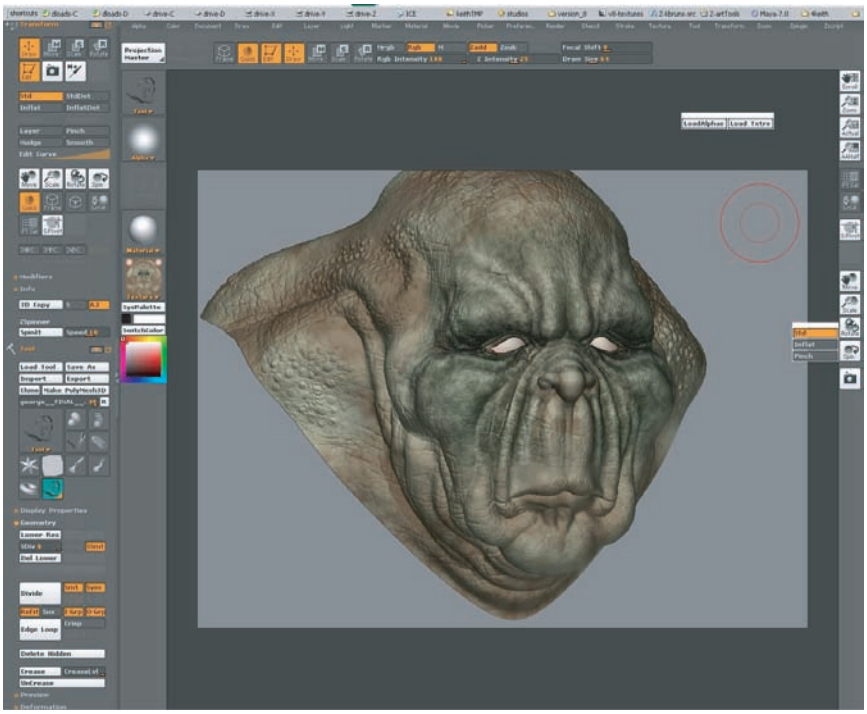

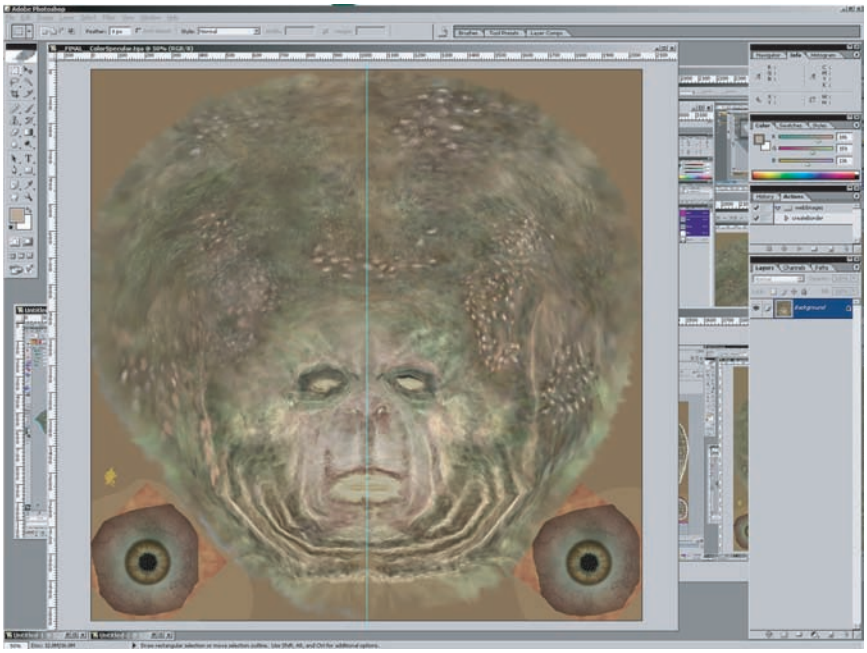

Plate XXXIX. Final version of the color texture from Plate XXXVII. *Image courtesy Keith Bruns.* (See also Figure 26.12.)

Plate XL. Rendering of the mesh with normal map and final color texture (from Figure 26.12) applied. *Image courtesy Keith Bruns.* (See also Figure 26.13.)

Plate XLI. Shader configuration in Maya. The interface on the right is used to select the shader, assign textures to shader inputs, and set the values of non-texture shader inputs (such as the “Specular Color” and “Specular Power” sliders). The rendering on the left is updated dynamically while these properties are modified, enabling immediate visual feedback. *Image courtesy Keith Bruns.* (See also Figure 26.14.)

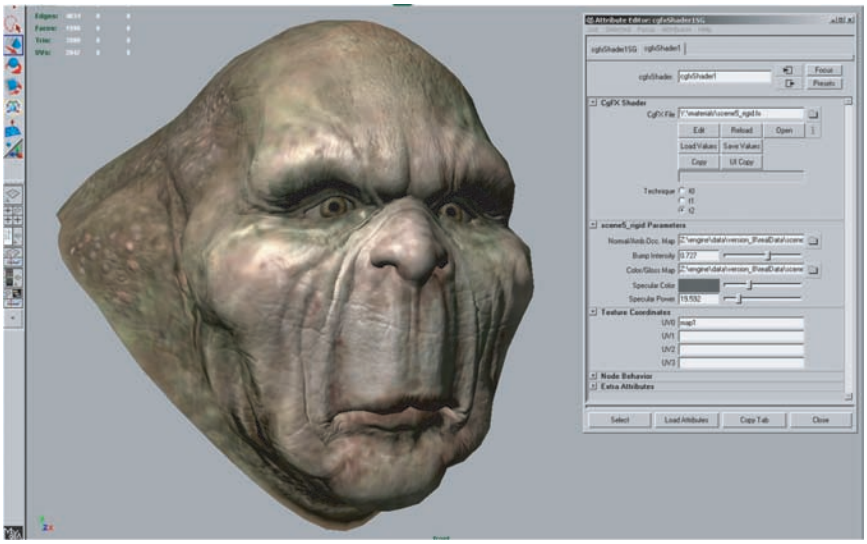

Plate XLII. The Tableau/Polaris system default mappings for four visual channels according to data type. *Image courtesy Chris Stolte* (Stolte et al., 2008), © 2008 IEEE. (See also Figure 27.6.)

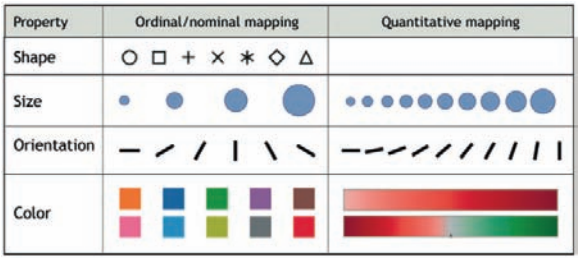

Plate XLIII. Complex glyphs require significant display area so that the encoded information can be read. *Image courtesy Matt Ward, created with the SpiralGlyphics software* (M. O. Ward, 2002). (See also Figure 27.14.)

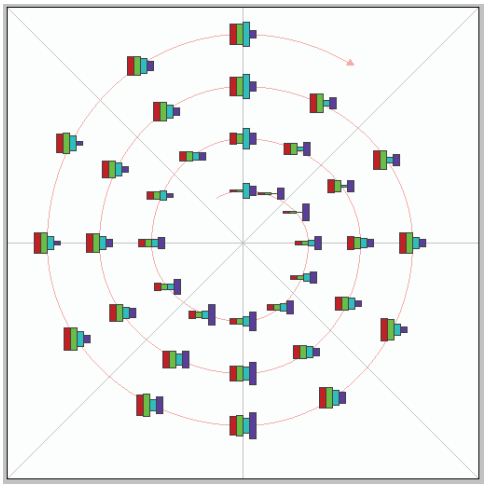

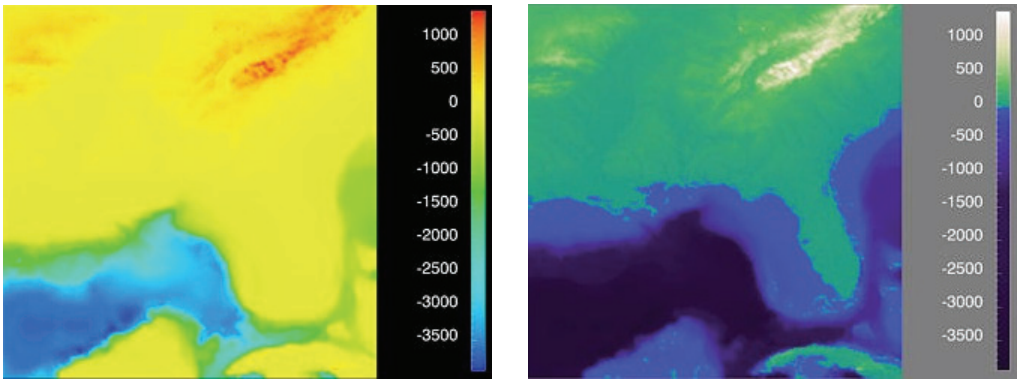

Plate XLIV. Left: The standard rainbow colormap has two defects: it uses hue to denote ordering, and it is not perceptually isolinear. (See also Figure 27.8.) Right: The structure of the same dataset is far more clear with a colormap where monotonically increasing lightness is used to show ordering and hue is used instead for segmenting into categorical regions. (See also Figure 27.9.) *Courtesy Bernice Rogowitz.*

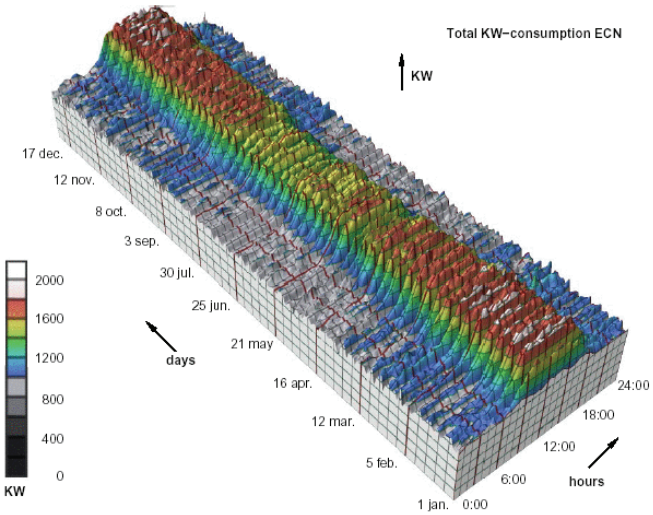

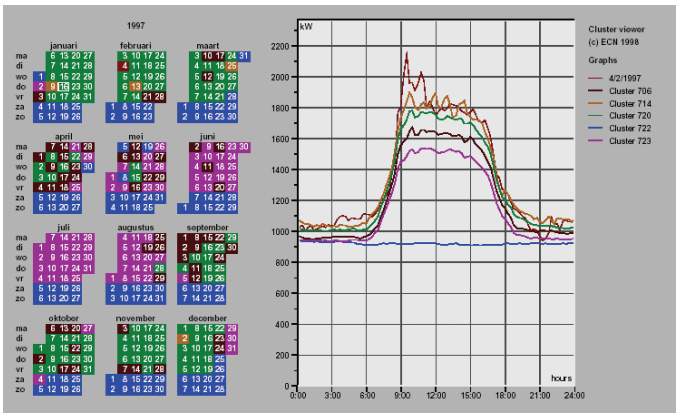

Plate XLV. Top: A 3D representation of this time series dataset introduces the problems of occlusion and perspective distortion. Bottom: The linked 2D views of derived aggregate curves and the calendar allow direct comparison and show more fine-grained patterns. *Image courtesy Jarke van Wijk* (van Wijk & van Selow, 1999), © 1999 IEEE. (See also Figure 27.10.)

Plate XLVI. Tarantula shows an overview of source code using one-pixel lines color coded by execution status of a software test suite. *Image courtesy John Stasko* (Jones et al., 2002), © 2002 ACM, Inc. Included here by permission. (See also Figure 27.11.)

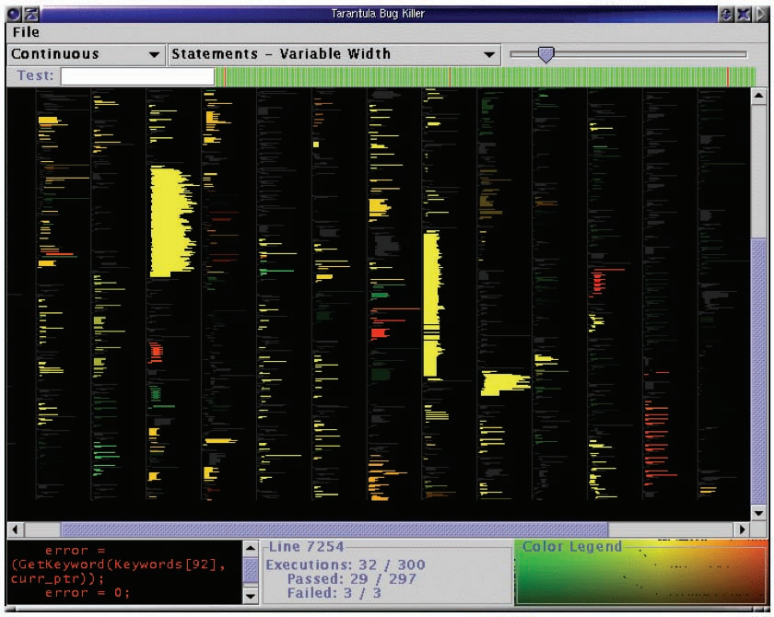

Plate XLVII. Visual layering with size, saturation, and brightness in the Constellation system (Munzner, 2000). (See also Figure 27.12.)

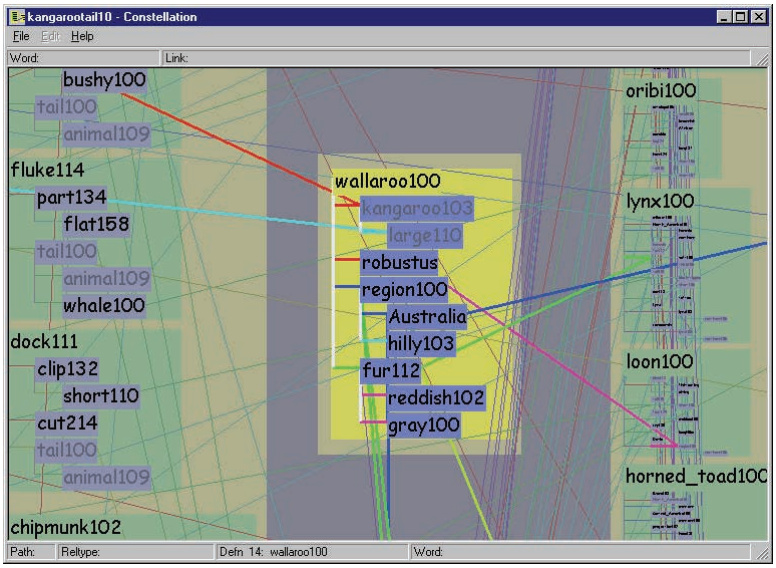

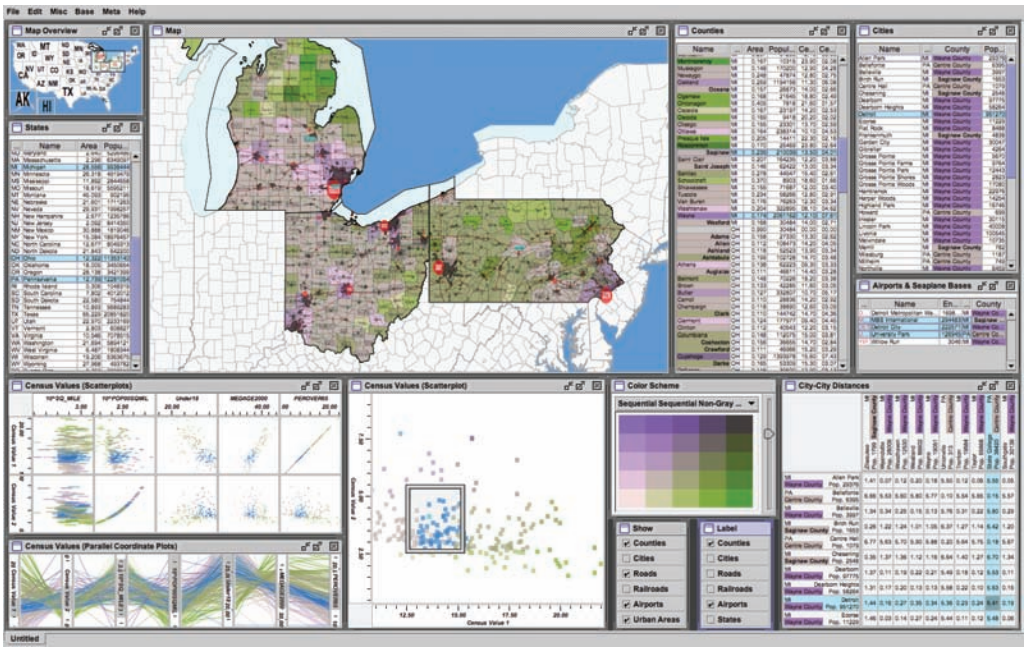

Plate XLVIII. The Improvise toolkit was used to create this multiple-view visualization. *Image courtesy Chris Weaver.* (See also Figure 27.16.)

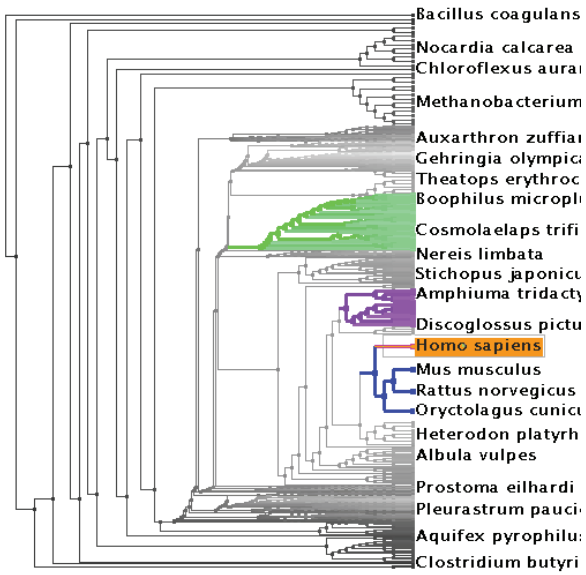

Plate XLIX. The TreeJuxtaposer system features stretch and squish navigation and guaranteed visibility of regions marked with colors (Munzner et al., 2003). (See also Figure 27.17).

Plate L. Dimensionality reduction with the Glimmer multidimensional scaling approach shows clusters in a document dataset (Ingram et al., 2009), © 2009 IEEE. (See also Figure 27.19.)

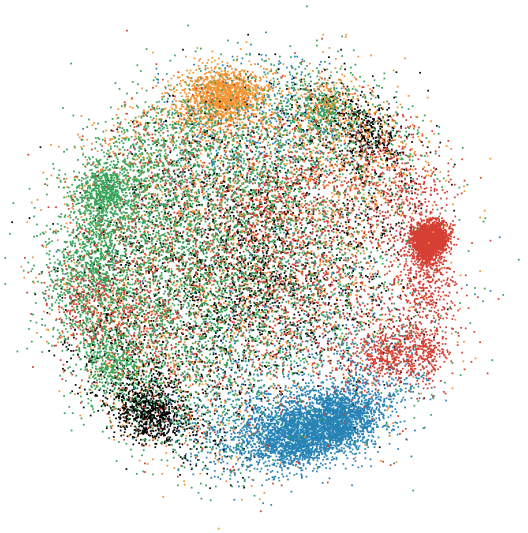

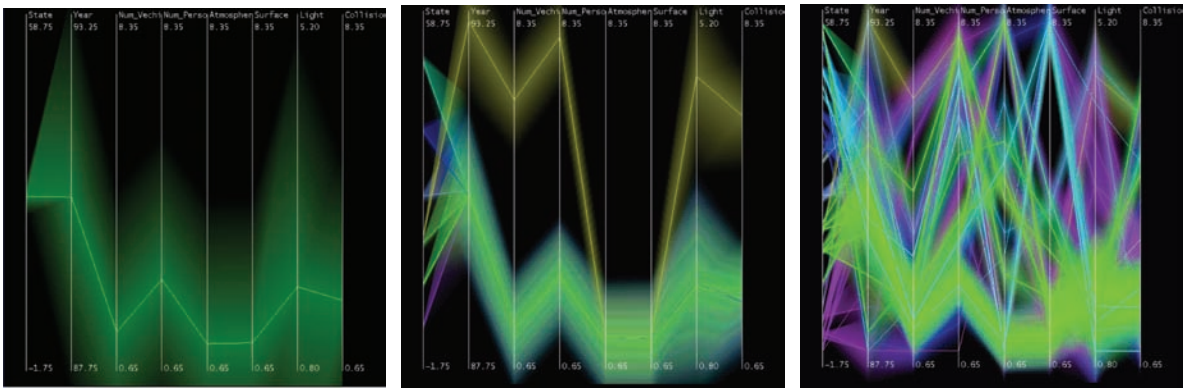

Plate LI. Hierarchical parallel coordinates show high-dimensional data at multiple levels of detail. *Image courtesy Matt Ward* (Fua et al., 1999), © 1999 IEEE. (See also Figure 27.21).

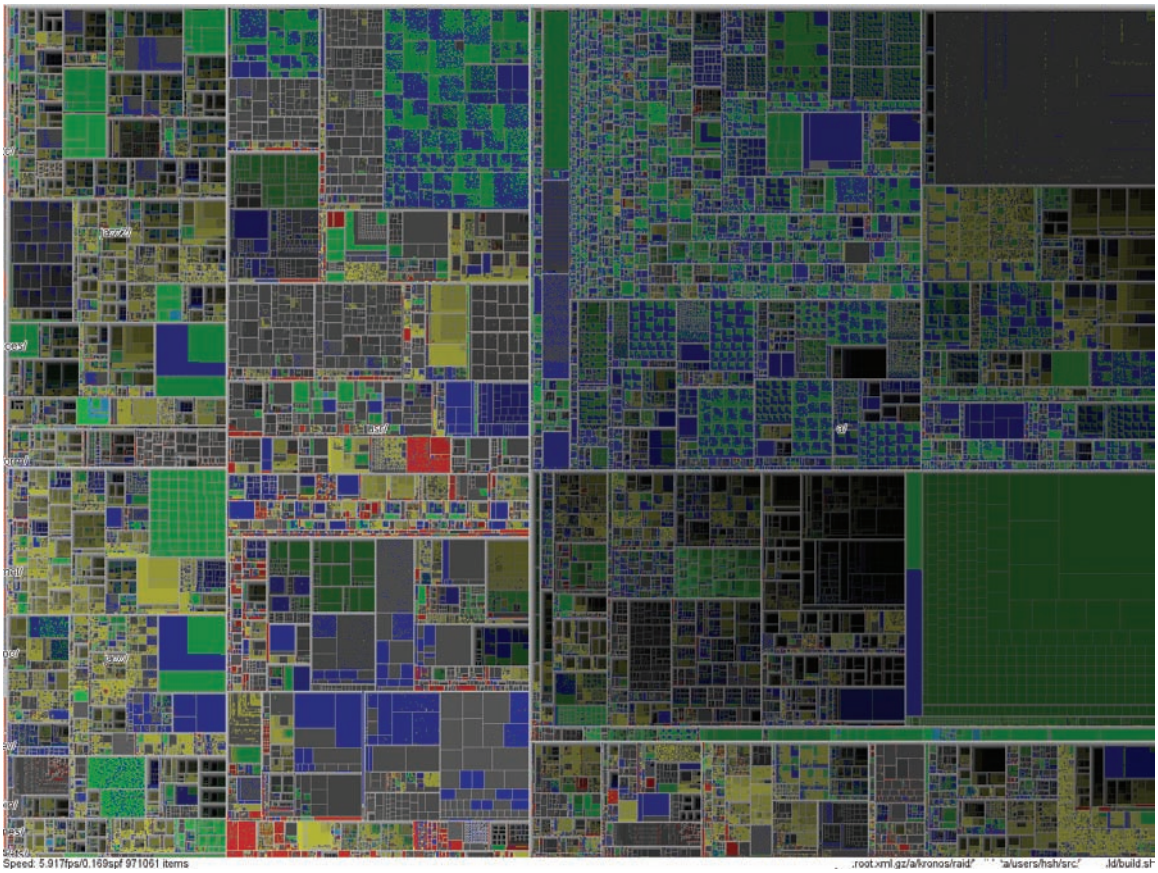

Plate LII. Treemap showing a filesystem of nearly one million files. *Image courtesy Jean-Daniel Fekete* (Fekete & Plaisant, 2002), © 2002 IEEE. (See also Figure 27.25.)

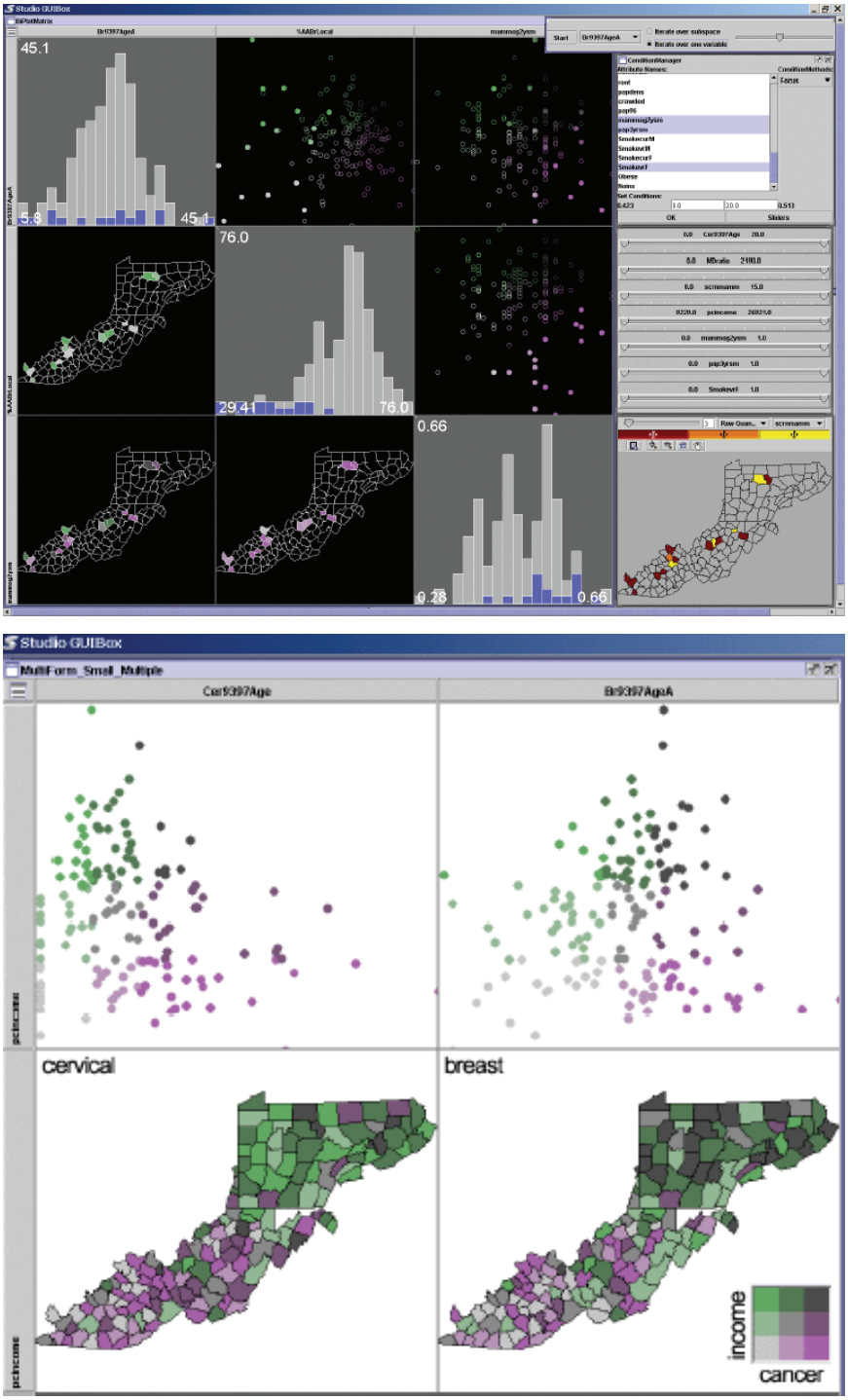

Plate LIII. Two matrices of linked small multiples showing cancer demographic data (MacEachren et al., 2003), © 2003 IEEE. (See also Figure 27.26).